European Journal of Medicinal Chemistry 83 (2014) 646–654

Contents lists available at ScienceDirect

European Journal of Medicinal Chemistry

journal homepage: http://www.elsevier.com/locate/ejmech

Original article

Curcumin-loaded guanidine functionalized PEGylated *I3ad* mesoporous silica nanoparticles KIT-6: Practical strategy for the breast cancer therapy

Leila Ma'mani [a], Safoora Nikzad [b], Hamidreza Kheiri-manjili [c], Sharafaldin al-Musawi [c], Mina Saeedi [a], Sonia Askarlou [d], Alireza Foroumadi [a], Abbas Shafiee [e, *]

[a] Pharmaceutical Sciences Research Center, Tehran University of Medical Sciences, Tehran 14176, Iran
[b] Department of Medical Physics, Faculty of Medical Sciences, Tarbiat Modares University, Tehran, Iran
[c] Department of Nanobiotechnology, Faculty of Biological Sciences, Tarbiat Modares University, Tehran, Iran
[d] Shahid Beheshti University of Medical Sciences, Tehran, Iran
[e] Department of Medicinal Chemistry, Faculty of Pharmacy and Pharmaceutical Sciences Research Center, Tehran University of Medical Sciences, Tehran 14176, Iran

ARTICLE INFO

Article history:
Received 29 March 2014
Received in revised form
27 June 2014
Accepted 28 June 2014
Available online 28 June 2014

Keywords:
Breast cancer
Curcumin
Drug delivery system
Guanidine functionalized PEGylated mesoporous silica nanoparticles
I3ad mesoporous silica nanoparticle KIT-6
pH sensitive

ABSTRACT

In this research, we have synthesized guanidine functionalized PEGylated mesoporous silica nanoparticles as a novel and efficient drug delivery system (DDS). For this purpose, guanidine functionalized PEGylated *I3ad* mesoporous silica nanoparticle KIT-6 [Gu@PEGylated KIT-6] was utilized as a promising system for the effective delivery of curcumin into the breast cancer cells. The modified mesoporous silica nanoparticles (MSNs) was fully characterized by different techniques such as transmission and scanning electron microscopy (TEM & SEM), N_2 adsorption-desorption measurement, thermal gravimetric analysis (TGA), X-ray powder diffraction (XRD), and dynamic light scattering (DLS). The average particle size of [Gu@PEGylated KIT-6] and curcumin loaded [Gu@PEGylated KIT-6] nanoparticles were about 60 and 70 nm, respectively. This new system exhibited high drug loading capacity, sustained drug release profile, and high and long term anticancer efficacy in human cancer cell lines. It showed pH-responsive controlled characteristics and highly programmed release of curcumin leading to the satisfactory results in *in vitro* breast cancer therapy. Our results depicted that the pure nanoparticles have no cytotoxicity against human breast adenocarcinoma cells (MCF-7), mouse breast cancer cells (4T1), and human mammary epithelial cells (MCF10A).

1. Introduction

Turmeric, *Curcuma longa* L. (Zingiberaceae family) rhizomes, is endowed with promising pharmaceutical properties and has a long history of medicinal uses in ancient for the treatment of a wide range of diseases. These medicinal properties are associated chiefly with curcumin, the compound presents in the rhizome of turmeric and chemically named (diferuloylmethane)-(1, 7-bis (4-hydroxy-3-methoxyphenyl)-1,6-hepadiene-3,5-dione) [1].

Currently, precious pharmaceutical properties of curcumin have been proved comprehensively [2] and the number of publications have endorsed its anti-oxidant [3], anti-cancer [4], anti-inflammatory [5], anti-microbial [6], and anti-fungal [7] activities. However, the most important point about the oral consumption of curcumin is related to its low bioavailability, demonstrated by Ravindranath and Chandrasekhara [8]. Curcumin is a hydrophobic polyphenol and insoluble in water, but is readily soluble in organic solvents such as dimethyl sulfoxide, acetone and ethanol. To take advantage of pharmaceutical activities of curcumin and overcome its poor availability at the site of action in the body, versatile approaches have been developed [9].

In recent decades, mesoporous silica nanoparticles (MSNs) has opened new horizon to introduce new DDSs and their efficiency have attracted a great deal of attention for their potential biomedical utilizes [10]. It is notable that, the proficiency of MSNs is indebted to the well-defined pores having a narrow diameter distribution, high pore volume, silanol functionalization opportunity, and specific surface area accompanied the hydrothermal stability

* Corresponding author.
E-mail address: ashafiee@ams.ac.ir (A. Shafiee).

http://dx.doi.org/10.1016/j.ejmech.2014.06.069
0223-5234/

[11]. Apart from these properties, the most outstanding aspect of MSNs is biocompatibility which has been proved in the *in vitro* and *in vivo* experiments leading to design of novel DDSs [12].

Another prospect which allows chemists to designate intelligent spacers for the efficient and controlled release of embedded drug is the feasibility of selective functionalization of MSNs. Literature review revealed that the convenient surface modification of different MSNs could be played crucial role in the improving their efficiency and intelligence as nano-DDSs [13]. Recently, MSNs with three-dimensional cubic *Ia3d* symmetry consisting of two interpenetrating continuous networks of chiral channels have shown lots of superiorities. Among 3*D* networks, KIT-6 which has composed of two interwoven nano-channels similar to that found in MCM-48 exhibited remarkable properties [14]. However; to the best of our knowledge only a few reports are available on the immobilization of biomolecules and drugs on organically modified KIT-6 [15].

PEG (poly ethylene glycol) is water soluble, FDA-approved, nontoxic, non-antigenic, non-immunogenic with no significant interfere with the drug release [16]. PEGylation of DDSs has been routinely used owing to their ability as an efficient manner to enhance the permeability, retention effect, blood circulation, EPR effect, and excellent colloidal stability in aqueous dispersions [17–22]. In this manner, various investigations were achieved to improve the drug delivery performance of different MSNs as DDSs by PEGylation [23–27]. With regard to these reports, the introduction of efficient and low-cost anticancer DDSs integrating three-dimensional cubic *Ia3d* MSNs with various surface characteristics would be of great significance. Therefore, focusing on the valuable medicinal properties of curcumin and in continuation of our successful experiences in the field of nanoporous materials [28]; herein, we present an efficient nano drug delivery system to enhance the absorption and therapeutic level of curcumin in the breast cancer. It was found that the guanidine functionalized PEGylated KIT-6 is a good candidate for the breast cancer treatment.

2. Material and methods

2.1. Chemicals, cell lines and cell culture

Pluronic P123 ($EO_{20}PO_{70}EO_{20}$), tetraethoxysilane (TEOS, 98%), 3-(4, 5-Dimethylthiazol-2-yl)-2,5-diphenyltetrazotium bromide (MTT), dimethyl sulfoxide (DMSO) and highly purified curcumin were purchased from Sigma Aldrich. Phosphate buffer (20 mM, pH 7.8), EDTA, and corresponding salts used in this research were purchased from Merck. Trypsin, culture medium (DMEM = Dulbecco's Modified Eagle's Medium), and supplements were obtained from Gibco (Germany). Human mammary epithelial (MCF10A), mouse breast cancer (4T1) and human breast adenocarcinoma (MCF-7) cell lines were obtained from Pasteur institute of Iran.

All cell lines were grown in DMEM medium supplemented with 10% (v/v) heat-inactivated fetal bovine serum (FBS), 2% L-glutamine, 2.7% sodium bicarbonate, 1% Hepes buffer, and 1% penicillin-streptomycin solution (GPS, Sigma) at 37 °C in humidified atmosphere with 5% CO_2. All cells were trypsinized in the solution of 0.05% trypsin and seeded into 96-well micro-plates at the density of 1×10^5 cells/well.

2.2. Characterization

The powder XRD spectrum was recorded at room temperature with a Philips X'pert 1710 diffractometer using CuKα (α = 1.54056 Å) in Bragg-Brentano geometry (θ-2θ). The morphologies of the products were observed using SEM (Hitachi S-4800 II, Japan) equipped with energy dispersive X-ray spectroscopy. The TEM experiments were performed on a Hitachi H-7650 (Tokyo, Japan) operating at an acceleration voltage of 80 kV. The IR spectra were taken using Nicolet FT-IR Magna 550 spectrographs with spectroscopic grade KBr. The surface areas were calculated by BET method and the pore size distributions were calculated from the adsorption branch of the isotherms using BJH method. The size of the nanoparticles was assessed by dynamic light scattering (Nano-ZS 90, Malvern Instrument, United Kingdom). The temperature was kept at 25 °C during the measuring process and measurements were recorded as the average of three test runs. The zeta potential of the nanoparticles was measured in folded capillary cells using Nanosizer (Zetasizer Nano ZS90, Malvern Instruments Ltd., Malvern, UK).

2.3. Preparation of guanidine functionalized PEGylated KIT-6, [Gu@PEGylated KIT-6]

2.3.1. Synthesis of KIT-6

KIT-6 was prepared according to the previous reported method [29]. A mixture of Pluronic P123 tri block copolymer and *n*-BuOH was used as structure-directing agents. The preparation of the KIT-6 proceeded as follows: 4.0 g of P123 was dissolved in 144 g of DI water and 7.9 g of 35 wt % HCl with stirring at 35 °C, and then 4.0 g of *n*-BuOH was added at once. After 1 h, 8.6 g of TEOS was added to this clear solution. This mixture was left under vigorous and constant stirring at 35 °C for 24 h. Subsequently, the temperature was increased to 100 °C and aged at the same temperature for 24 h under static condition. The white precipitate product was filtered without further washing and dried under vacuum at 100 °C overnight. The template was removed via a brief EtOH/HCl washing after calcination at 550 °C for 6 h.

2.3.2. Synthesis of [PEGylated KIT-6]

PEG_{600}–silane was synthesized via the hydrogen-transfer nucleophilic addition reaction between the end hydroxyl group of PEG (MW = 600) and the isocyanate group of 3-(triethoxysilyl) propyl isocyanate (TESPIC) [25]. The probable adsorbed water in purchased PEG was removed at 90 °C for 3 h in vacuum. Then 0.01 mol of dried PEG_{600} were completely dissolved into 50 mL of dry pyridine with vigorous stirring under argon atmosphere at 70 °C. After stirring for 6 h, 0.01 mol of TESPIC was added into the aforementioned mixed solution. After 24 h, the solvent was removed by vacuum evaporation. The residue was washed three times with *n*-hexane, and then recrystallized from EtOH at 0 °C. The obtained white waxen PEG_{600}–silane was filtered at 0 °C, and then dried at room temperature in vacuum. Then a solution of 0.1 g of PEG_{600}–silane in 30 mL of EtOH was added drop-wise to a vigorous stirring solution of 25 mg of as-prepared KIT-6 in 30 mL EtOH/H_2O (1:2) and HCl (pH = 4). After vigorous stirring for 24 h, the solution was filtered off and washed thoroughly. The white residue was dried at 100 °C in vacuum for 12 h to achieve [PEGylated KIT-6].

2.3.3. Synthesis of [Gu@PEGylated KIT-6]

4 mmol aminopropyltriethoxysilane (APTES) was added to a suspension of 1 g of the previously [PEGylated KIT-6] in 30 mL toluene. The suspension was gently stirred for 24 h under reflux condition. The suspension was filtered off, washed and finally dried under vacuum exhaustively to obtain aminopropyl functionalized PEGylated KIT-6 [H_2N-nPr-PEGylated KIT-6]. Then, [Gu@PEGylated KIT-6] was prepared by stirring 0.5 g of [H_2N-*n*Pr-PEGylated KIT-6] with 0.3 g (2.0 mmol) of 1-*H*-pyrazole-1-carboxamidine hydrochloride and 0.36 mL (2.1 mmol) diisopropyl ethylamine in 5 mL of

DMF for 24 h. The resulting fine powder was centrifuged, washed with EtOH and dried under vacuum for 20 h.

2.3.4. Drug loading into the surface of [Gu@PEGylated KIT-6]

To load CUR into the functionalized surface of the pores of nanocarrier, a curcumin solution in acetone (3.0×10^{-3} M) was added drop-wise to a 5 mg of [Gu@PEGylated KIT-6] and lived for 24 h under inert atmosphere. Finally the solid was centrifuged at 15,000 rpm for 5 min. Then, the collected solid was washed thoroughly with EtOH (30 mL) to rinse away any surplus curcumin and dried under vacuum to achieve curcumin loaded [Gu@PEGylated KIT-6] which was denoted as CUR@[Gu@PEGylated KIT-6] [30]. To evaluate the CUR-loading efficiency, the supernatant and washed solutions were collected and the residual CUR content was measured by using UV–vis measurement. The loading content (LC %) and loading efficiency (LE %) of CUR can be calculated as follows:

$$\text{SF loading content}(\%) = \frac{\text{Weight of SF in MSN}}{\text{Weight of MSN}} \times 100\% \quad (1)$$

$$\text{SF loading efficiency}(\%) = \frac{\text{Weight of SF in MSN}}{\text{Weight of Free SF}} \times 100\% \quad (2)$$

2.4. Analysis of loaded drug

2.4.1. Fluorescence stability

The fluorescence emission of curcumin was analyzed in diverse biological medium to assess the capability and efficacy of the prepared [Gu@PEGylated KIT-6] nanoparticles in drug protection. To this purpose, ammonium buffer 20 mM (pH = 9.25), phosphate buffer 20 mM (pH = 7.40), acetate buffer 20 mM (pH = 4.75), and cell culture Dulbecco's Modified Eagle's Medium (DMEM; pH = 7.40) were prepared. Then CUR@[Gu@PEGylated KIT-6] were dispersed directly in the mediums at a concentration of 25 μg mL^{-1} (drug content equal to 5.43 μM). In addition, [Gu@PEGylated KIT-6] and curcumin at the same concentration was used as a reference. The fluorescence emission spectra were recorded from 420 to 700 nm.

2.4.2. In vitro drug release profile

1 mg of the CUR loaded [Gu@PEGylated KIT-6] was poured into a dialysis bag (Spectrapor, MW cutoff 3500 g mol^{-1}) and put into 500 mL of phosphate buffer solution (PBS) (0.01 M, pH = 7.4) and citrate buffer (0.01 M, pH = 5.4). The release assay was performed at 37 °C using a shaking water bath (GFL, Burgwedel, Germany). Sampling was performed at 0, 4, 8, 12, 24, 48, 72, 96, and 120 h according to the sink condition. In each time point, 1 mL of the sample was drawn out, freeze dried and dissolved in 2 mL of methanol. Then, the samples were evaluated using fluorescence spectroscopy to determine the quantity of the releasing curcumin. To facilitate the exact estimation of the amount of curcumin released from CUR@[Gu@PEGylated KIT-6], an identical standard of curcumin (0–10 μg/mL) was prepared and the absorbance was measured at 450 nm using the UV–vis spectrometer. The accumulated release was calculated using the following equation:

$$R = \frac{V\sum_{i}^{n-i} C_i + V_0 C_n}{m_{\text{drug}}}$$

Eq. (1). The equation to calculate the accumulated release of CUR from CUR@[Gu@PEGylated KIT-6].

Where, R is the accumulated release (%), V is the sampling volume, V_0 is the initial volume, C_i and C_n are the curcumin concentrations, i and n are the sampling times, and m_{drug} is the mass of loaded curcumin into [Gu@PEGylated KIT-6].

2.4.3. Cell cultures and in vitro experiments

The human breast adenocarcinoma cell line (MCF-7) was kept in DMEM F12 medium, supplemented with 10% FBS and 2 mM L-glutamine and grown at 37 °C in a 5% CO_2 atmosphere. For each run, the dried CUR@[Gu@PEGylated KIT-6] nanoparticles were re-suspended in the complete culture medium to give the final concentration of 10–60 μM, and then added to the cells. Stock solution of curcumin (100 mM) were prepared in DMSO and diluted with the culture medium to get the same amount of curcumin carried by [Gu@PEGylated KIT-6] nanoparticles.

2.4.4. Determination of nanoparticles cytotoxicity

To rule out the toxicity of [Gu@PEGylated KIT-6] and CUR@[Gu@PEGylated KIT-6] NPs, MTT assay was accomplished. The cells (in culture medium) were dispensed in 96-well plates (100 μL in each well containing 1×10^5 cells per well) for overnight till the cells adhered to the wells. Then, the media was changed with prepared concentrations of nanoparticles (included [Gu@PEGylated KIT-6], [PEGylated KIT-6], [KIT-6], and CUR@[Gu@PEGylated KIT-6] NPs) which dissolved in culture medium with the range of 10–60 μM. After 24, 48, and 72 h of exposure, the toxicity was monitored by adding tetrazolium salt (4 h incubation). Afterward, upper media were gently removed from all wells using a syringe and 100 μL of DMSO were added to each wells and were shake on an Eppendorf Thermo-mixer at 37 °C and 1200 rpm to dissolve all crystals, after 10 min the samples were transferred to the ELISA reader (power wave 300, Biotek, USA) and the optical density was read using a test wavelength of 570 nm and a reference (background absorbance subtraction) wavelength of 690 nm.

2.4.5. Apoptosis measurement

Apoptosis was detected using Annexin V-FITC apoptosis detection Kit (Biovision, Inc.) and analyzed by flow cytometry. MCF-7 Cell lines were seeded in 6-well plates (1.0×10^5 cells per well) and 24 h after plating, were incubated with 100 μg mL^{-1} CUR@[Gu@PEGylated KIT-6] nanoparticles for 12, 24 and 48 h or left untreated as control. Next, the cells were washed twice with cold PBS, then carefully trypsinized to avoid mechanical damage of the membrane and re-suspended in Annexin binding buffer in the presence of Annexin V–FITC and propidium iodide (PI) stain. The sample acquisition was performed using the flow cytometer (BD Bioscience FACS, USA).

3. Results and discussion

3.1. Preparation and characterization of drug delivery system

The modified mesoporous solids including [Gu@PEGylated KIT-6] and CUR@[Gu@PEGylated KIT-6] were prepared as shown in Scheme 1. The prepared nanoparticles were comprehensively characterized by XRD, N_2 adsorption-desorption analysis, FT-IR, TGA, TEM, and SEM. SEM and TEM were applied to recognize the structural order and morphology of the pure mesoporous solid KIT-6 (Fig. 1). As shown in TEM images, the synthesized KIT-6 possesses an ordered cubically honeycomb-like network with uniform nanochannels. The average pore diameters of the KIT-6 which estimated from the TEM images, was about 7.5 nm, well agreeing with that from the XRD patterns and N_2 sorption analysis.

To confirm the ordered mesoporous frameworks, the XRD experiment utilized as a very sensitive and applicable technique.

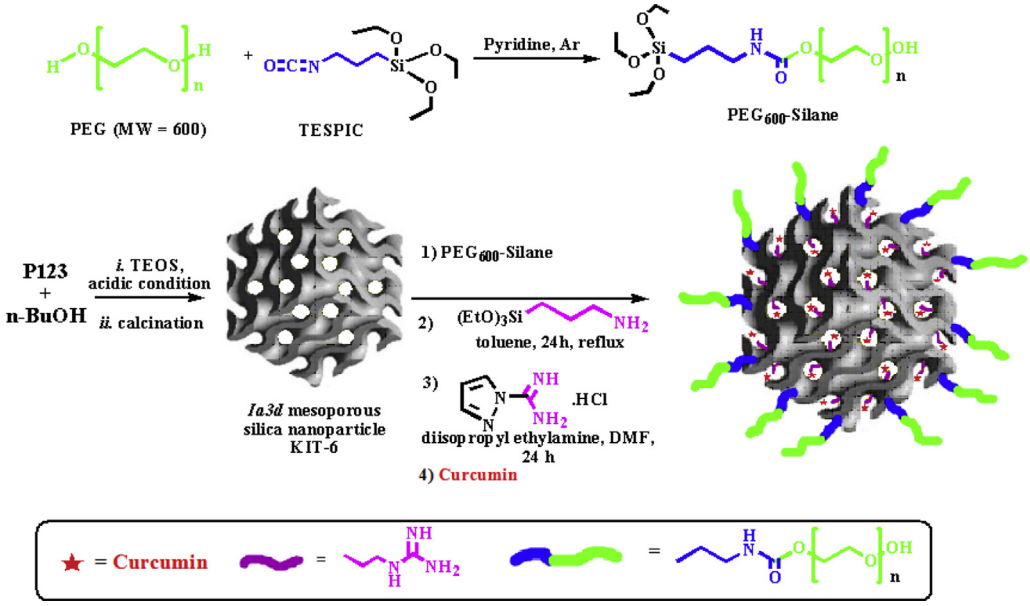

Scheme 1. The synthesis of CUR@[Gu@PEGylated KIT-6].

The XRD patterns are shown in Fig. 2, and clearly are attributable to the corresponding reflections of the 3*D* cubic symmetry of the space group Ia_3d. As shown, the sharp peak along with a distinct shoulder peak due to the 211 and 220 diffractions has appeared at $2\theta = 0.88^\circ$ and $2\theta = 0.96^\circ$, respectively. Another low intense diffraction peak of higher order has appeared at $2\theta = 1.67^\circ$, indicating (332) reflection. Except for the expected decrease in the peaks intensity, no significant changes were observed during the post modification processes. The positions of XRD peaks remained virtually fixed which proved the retention of the mesoporous structure of KIT-6 after functionalization. These XRD diffractograms generally confirmed that [Gu@PEGylated KIT-6] were successfully prepared for the desirable potential applications.

To quantify the porous nature of the particles, the N_2 adsorption–desorption isotherm experiment was carried out. It has revealed a high pore volume and surface area in the synthesized KIT-6 (Fig. 3). The specific surface area of the calcined KIT-6 was calculated by the multiple-point BET (Barrett–Joyner–Halenda) around 834.61 $m^2\ g^{-1}$. And its pore diameter distribution was determined using BJH (Barrett–Joyner–Halenda) averaged ~7.5 nm

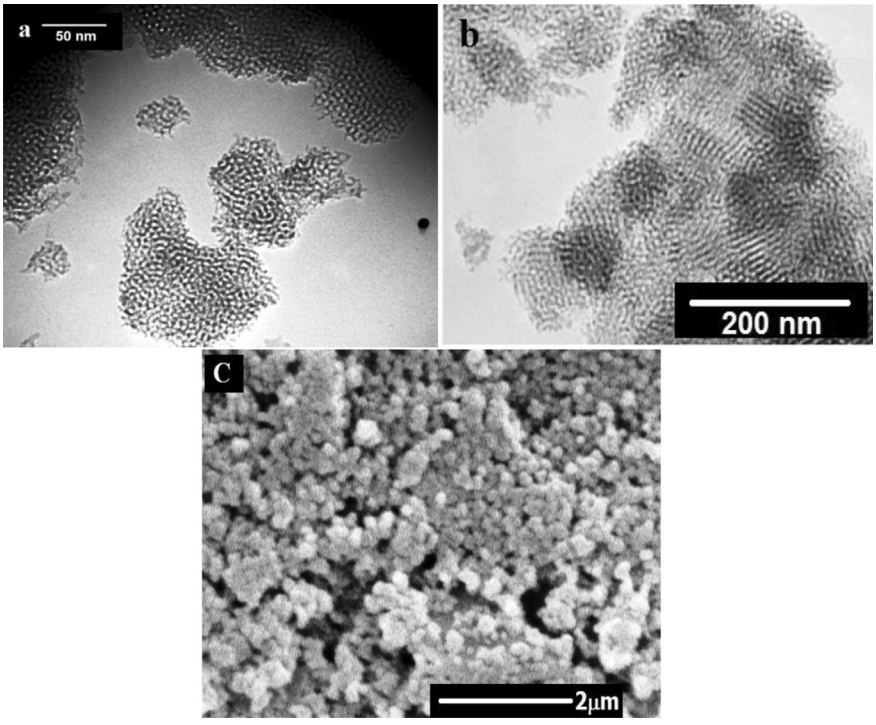

Fig. 1. TEM image (a), (b); and SEM image (c) of *I3ad* Mesoporous Silica Nanoparticles KIT-6.

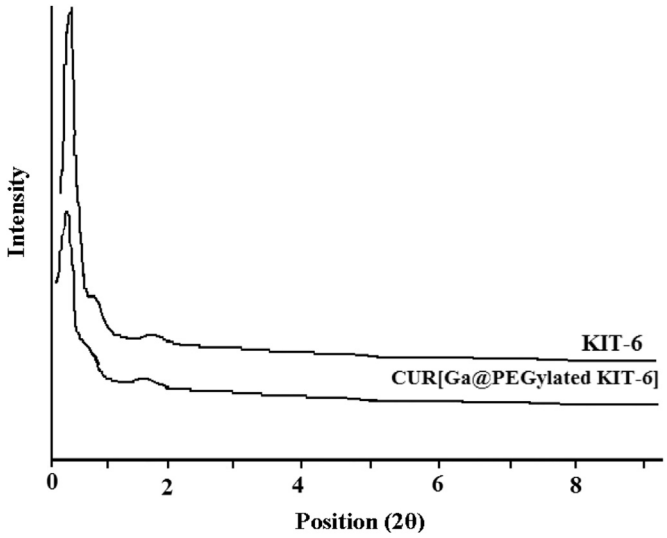

Fig. 2. The XRD patterns of KIT-6 and CUR@[Gu@PEGylated KIT-6].

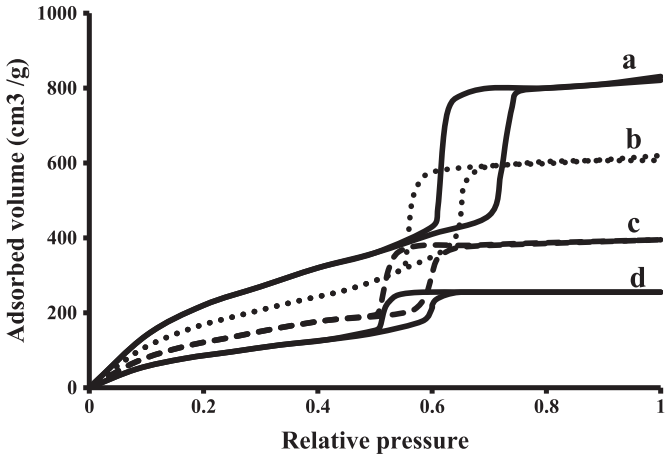

Fig. 3. N_2 adsorption/desorption isotherm of a) KIT-6, b) [PEGylated-KIT-6], c) [Gu@PEGylated KIT-6], d) CUR@[Gu@PEGylated KIT-6].

and total pore volume ~1.81 $cm^3\ g^{-1}$. Based on these results, the surface area, pore volume, and pore size of functionalized KIT-6 samples were decreased (Table 1). Despite the decrease in the adsorbed amount of N_2, the shape of the hysteresis loop was typically identical. This observation has confirmed that the pore shape might not be significantly changed during the silane functionalization and post modification process to prepare [Gu@PEGylated KIT-6].

The presence of the guanidine and PEG groups on the mesoporous framework after functionalization of KIT-6 and also the successful immobilization of curcumin were confirmed by FT-IR spectra (Fig. 4). The spectrum of [Gu@PEGylated KIT-6] exhibited new peaks indicating the changes in the structure of KIT-6. As shown in Fig 4b, after the reaction between PEG_{600}–silane and KIT-6, the resultant [Gu@PEGylated KIT-6] did not show any vibration at 2000–2500 cm^{-1} which confirmed the absence of the isocyanate group. Meanwhile, two bands appeared at 1712 cm^{-1} and 1530 cm^{-1} which should be assigned to the carbonyl and amide vibrations in –NHCOO– group, respectively. Moreover, another two bands appeared at 1130 cm^{-1} and 780 cm^{-1}, which are assigned to Si–O–Si and C–Si vibrations in silanes, respectively. The another bands which appeared at 1667 cm^{-1} and 1430 cm^{-1}, are assigned to guanidyl and C–N vibrations, respectively.

In Fig. 5, the TGA analysis of [Gu@PEGylated KIT-6] showed a first peak at 95 °C and second peak at 395 °C which related to the desorption of water and loss of the organic spacer group, respectively. Therefore, we can conclude that the loading of PEG was 20% and the loading of guanidine functional onto KIT-6 was 25% (~2.0 mmol g^{-1}). The loading of guanidine functional onto KIT-6 was also confirmed by acid-base back titration and elemental analysis. Also in the case of CUR@[Gu@PEGylated KIT-6], the TGA analysis showed the weight loss about 89%, which is attributed to the removal of curcumin, guanidine and PEG groups. Based on these results, we found that the loading of the curcumin moiety was 1.67 mmol g^{-1} of [Gu@PEGylated KIT-6].

The dynamic light scattering (DLS) and zeta-potential measurements have also been carried out to determine the size distribution and surface charges of the non-modified and modified NPs .The zeta potential, which arises from the existence of charge on the particle surfaces, is the electrostatic potential at the slipping plane in the electrical double layer separating the thin layer of liquid bound to the matrix surface. The reported zeta potential for non-functionalized KIT-6-type MSNs is highly negative as expected from the low isoelectric point (pH = 2–3) of pure silica. In comparison, zeta potential measurements showed that the negatively charge of MSNs became slightly positively charged (3.3 mV) after PEGylation, and the existence of guanidine in the nanoparticles of [Gu@PEGylated KIT-6] is reflected by a strongly positive zeta potential of the particles, i.e. 24 ± 5 mV which arises from the fully ionization of the guanidine groups at physiological pH (Fig. 6a, b). Particle size distribution of PEGylated KIT-6-type MSNs and [Gu@PEGylated KIT-6] in PBS solution measured by DLS is relatively narrow particle size distribution (mean dimmer = 64.06 ± 15.2,

Table 1
BET and BJH analysis before and after functionalization.

Mesoporous material	S_{BET} ($m^2\ g^{-1}$)	V_{total} ($cm^3\ g^{-1}$)	Pore diameter (nm) (BJH)
KIT-6	834.61	1.81	7.5
[PEGylated-KIT-6]	595.6	0.485	5.7
[Gu@PEGylated KIT-6]	355.3	0.398	3.9
CUR@[Gu@PEGylated KIT-6]	234.6	0.219	2.1

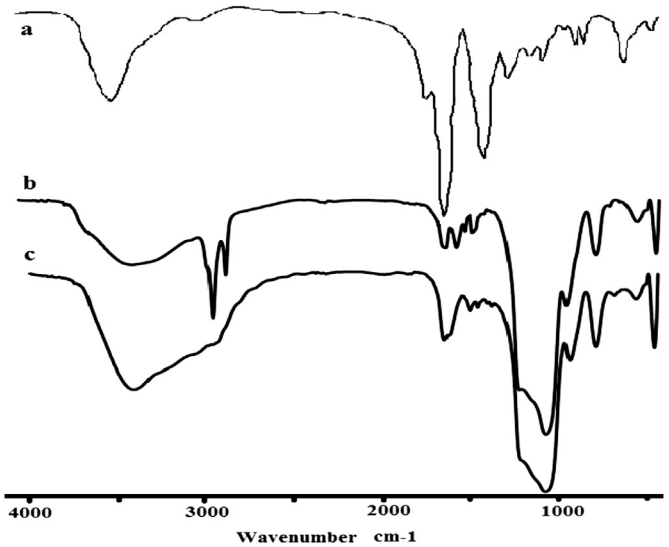

Fig. 4. FT-IR spectra of a) curcumin, b) [Gu@PEGylated KIT-6], and c) CUR@[Gu@PEGylated KIT-6].

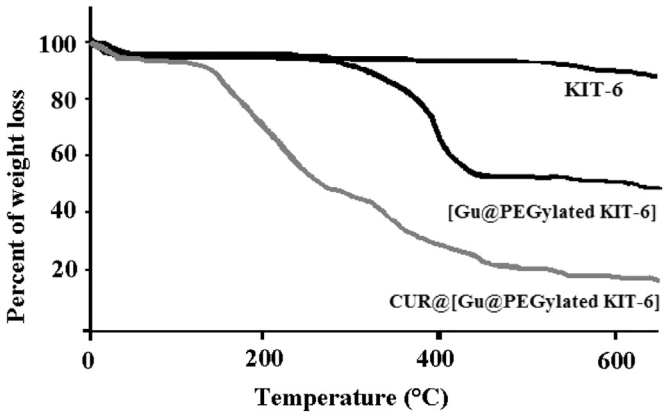

Fig. 5. TGA analysis of KIT-6, [Gu@PEGylated KIT-6], and CUR@[Gu@PEGylated KIT-6].

PDI = 0.025) and same measurements for [Gu@PEGylated KIT-6] showed mean dimmer = 68.85 ± 21.62 PDI = 0.065 (Fig. 6c, d). Therefore, the DLS and TEM data indicate that this polymer coating procedure can avoid the agglomeration of the nanoparticles into the larger (micrometer-scale) aggregates, which is a critical factor in biomedicine applications.

As it is known, the affinity of the guanidine functional groups to carbonyl functional groups in curcumin can form the CUR@[Gu@PEGylated KIT-6] complex by the electrostatic interaction, which can enhance the loading of drug into the MSN's pores. We first investigated the drug-loading capacity of the [Gu@PEGylated KIT-6] by determining the total amount of loaded drug. We then determined the loading content (LC %) of CUR at different weight ratios of CUR/[Gu@PEGylated KIT-6]. The maximum LC% of 50% is reached at the CUR concentration of 1.0 mg mL^{-1}.

Finally, the efficacy and capability of [Gu@PEGylated KIT-6] NPs were investigated in the releasing of curcumin, under different pH conditions including phosphate buffer (0.01 M, pH = 7.4) and citrate buffer (0.01 M, pH = 5.4) at 37 °C [31]. The amount of released curcumin from [Gu@PEGylated KIT-6] NPs was determined by measuring the fluorescence emission intensity of the supernatant at different pH values. As shown in Fig. 7 the profiles of the release process were expressed based on the weight percentages of curcumin at the different pH values. According to the release curves, curcumin release from the nanoparticles over a 96 h period and this time was slower at pH = 7.4 in comparison to pH = 5.4, and in the comparison with the release profiles of free curcumin, there are similar release profiles at pH = 7.4 and 5.4. Under the studied conditions, in 48 h 41.19% and 82.26% of loaded curcumin was released at pH = 7.4 and 5.4, respectively. After 72 h, 45.23% and 97.75% and after 120 h, 52.41% and approximately 100% of loaded curcumin was released at pH = 7.4 and 5.4, respectively. These results strongly indicated that the acidic protons effectively cleaved the hydrogen bonds between curcumin and the guanidyl group attached onto the surface of MSN. As a result, the pH values of the medium has pivotal role in the release rate of curcumin from

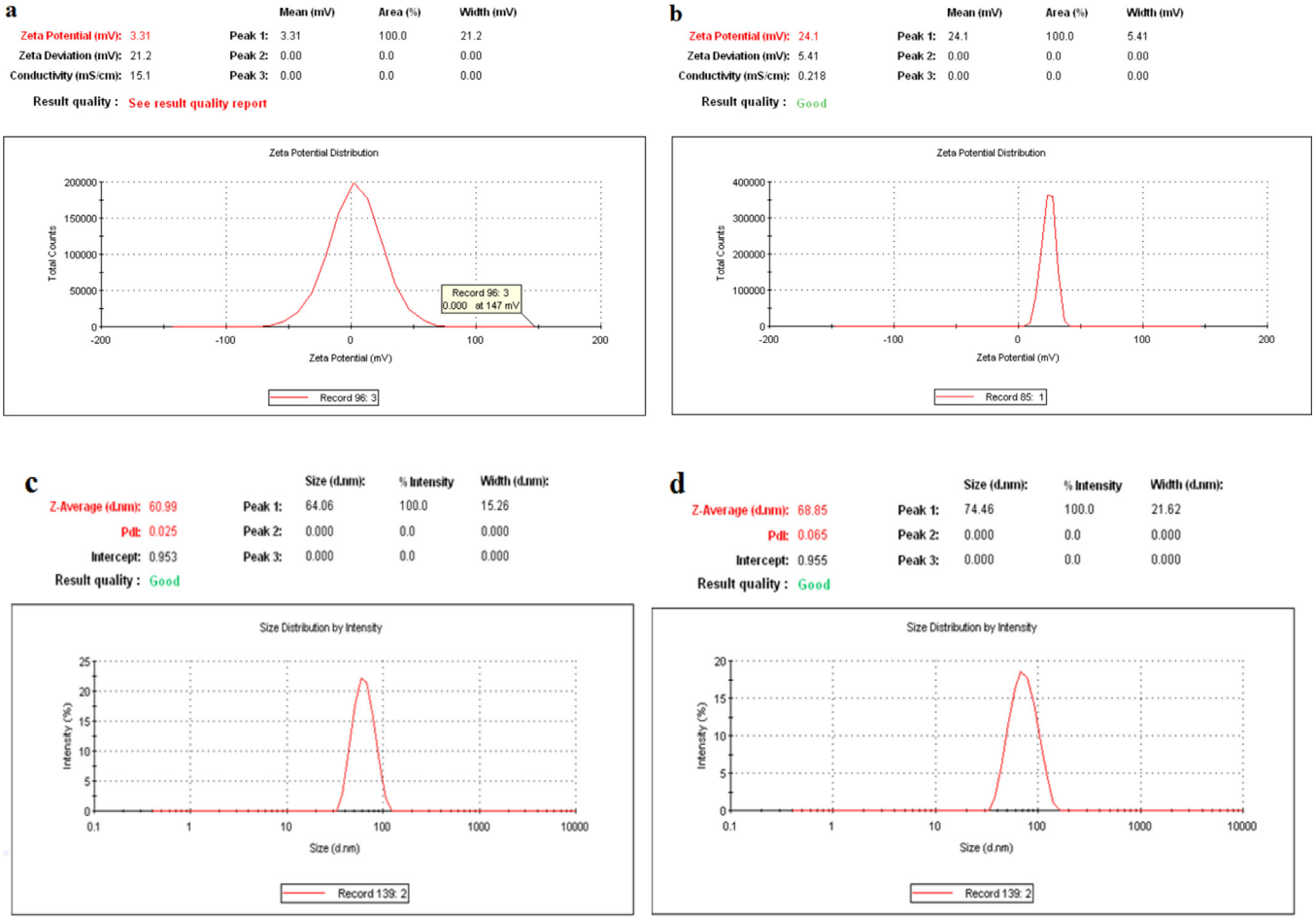

Fig. 6. The zeta-potentials of a) PEGylated KIT-6, b) [Gu@PEGylated KIT-6]; and DLS of c) PEGylated KIT-6, and d) [Gu@PEGylated KIT-6].

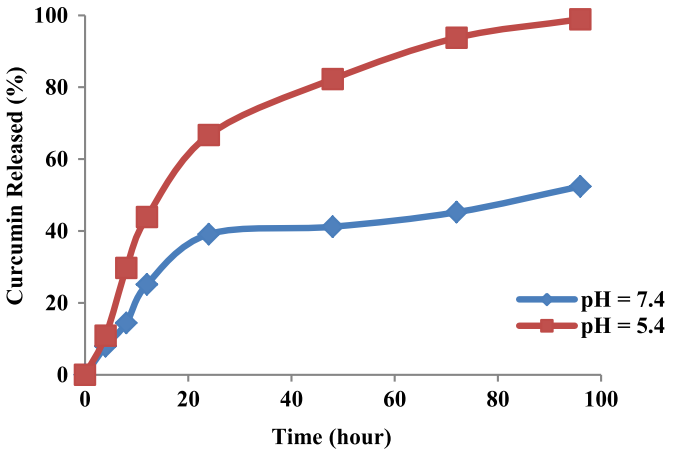

Fig. 7. *In vitro* release profiles of CUR@[Gu@PEGylated KIT-6] at pH 7.4 and pH 5.4; all experiments were performed at 37 °C. Data represent mean values ± SD ($n = 3$).

[Gu@PEGylated KIT-6]. It is notable that the amount of curcumin released from Cur@[Gu@PEGylated KIT-6] can be efficiently controlled by the acidity of medium.

We originally determined the toxicity of curcumin on MCF7 and 4T1 cancerous cell lines as well as human mammary epithelial (MCF10A). As shown in Fig. 8, CUR@[Gu@PEGylated KIT-6] significantly suppresses the proliferation of MCF7 and 4T1 cancerous cell lines in a dose and time-dependent manner in comparison with the pure curcumin and [Gu@PEGylated KIT-6] NPs ($Pb < 0.01$). The IC_{50} value of CUR@[Gu@PEGylated KIT-6] for MCF7 cell lines within 24 h were 27.4 μM which reduced to 19.5 μM in 48 h. The IC_{50} values of CUR@[Gu@PEGylated KIT-6] for 4T1 cells were slightly different and were equal to 29.11 μM for 24 h and decreased to 14.68 μM for 48 h. In contrast, the same concentrations of CUR@[Gu@PEGylated KIT-6] did not affect the proliferation of MCF10A cells. Furthermore, [Gu@PEGylated KIT-6], [PEGylated KIT-6], and [KIT-6] NPs did not show any side effects on the cell lines even at concentration of 60 μM, which in turn confirms the safety use of these nanoporous materials on the mouse and human cell lines. The experiments were separately done in triplicate for the three cell lines.

To determine the cytotoxic effect of CUR@[Gu@PEGylated KIT-6] NPs on MCF-7 cells, flow cytometry was performed at 12, 24 and 48 h after treatments. The percentage of live cells (A^-/PI^-) was 89.0% after 12 h significantly decreased to 73.2% after 24 h and 7.62% after 48 h which indicates the powerful cytotoxicity of designed curcumin loaded nanoparticles. Apoptosis rate for early apoptosis (A^+/PI^-) was 9.97%, 20.0% and 69.8% at 12, 24 and 48 h, respectively and it was 0.878%, 2.53% and 17.4% for late apoptosis (A^+/PI^+). These results suggested that rate of total apoptosis significantly increased by passing time and this increase is more considerable in the case of early apoptosis which proves the effective function of NPs in modifying the cytotoxic effects of curcumin. Percentage of necrotic cells (A^-/PI^+) was also increased at hour 48 in comparison to hours 24 and 12 (Fig. 9).

3.2. Cell internalization

In order to cell internalization study of CUR@[Gu@PEGylated KIT-6] and free curcumin, MCF-7 cells were plated in 100 mm

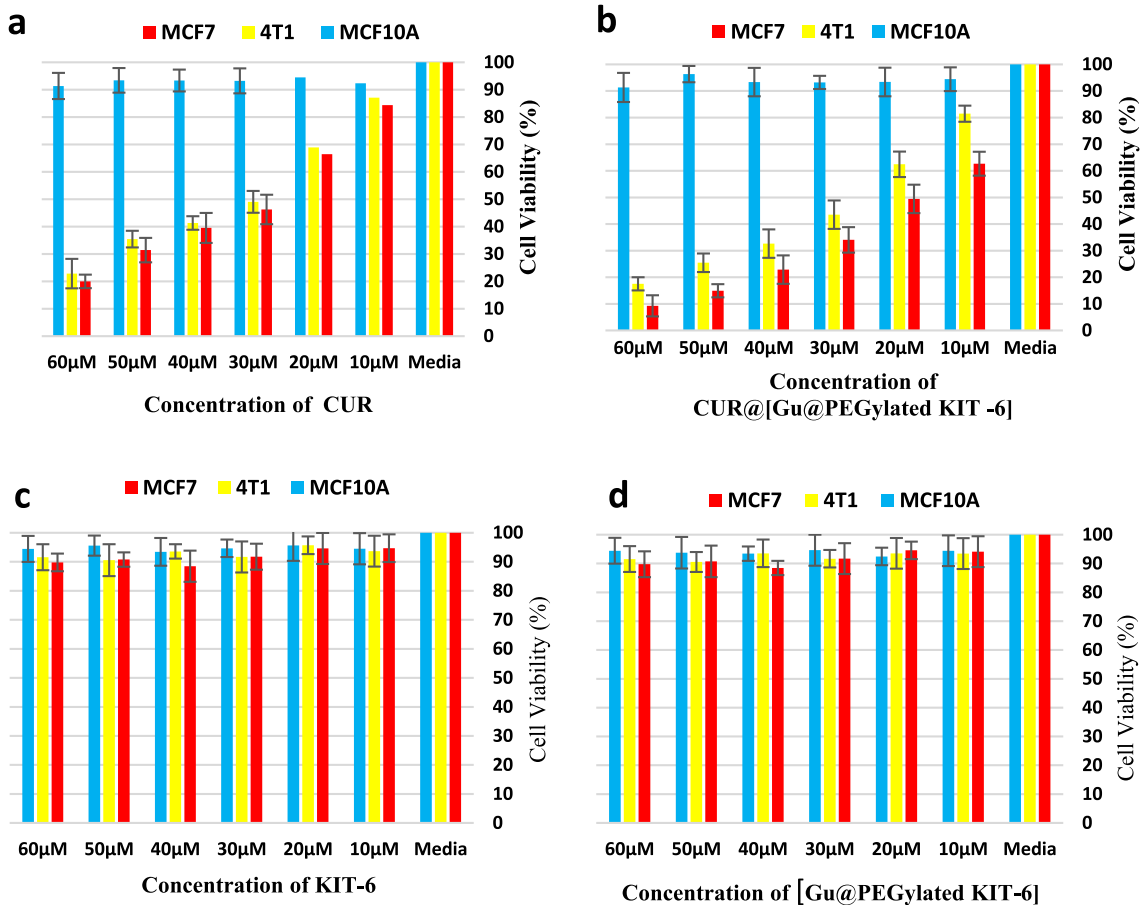

Fig. 8. The cytotoxicity effects of a) curcumin, b) CUR@[Gu@PEGylated KIT-6], c) KIT-6, and d)[Gu@PEGylated KIT-6] on the cancerous and normal cells (MCF7, 4T1 and MCF10A) were measured.

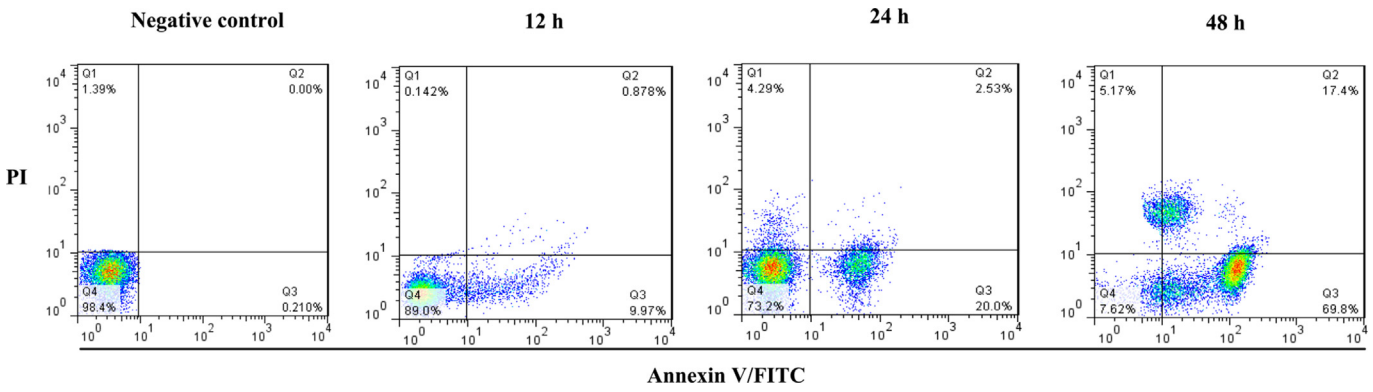

Fig. 9. The apoptosis induction by CUR@[Gu@PEGylated KIT-6] on **MCF7** cell line.

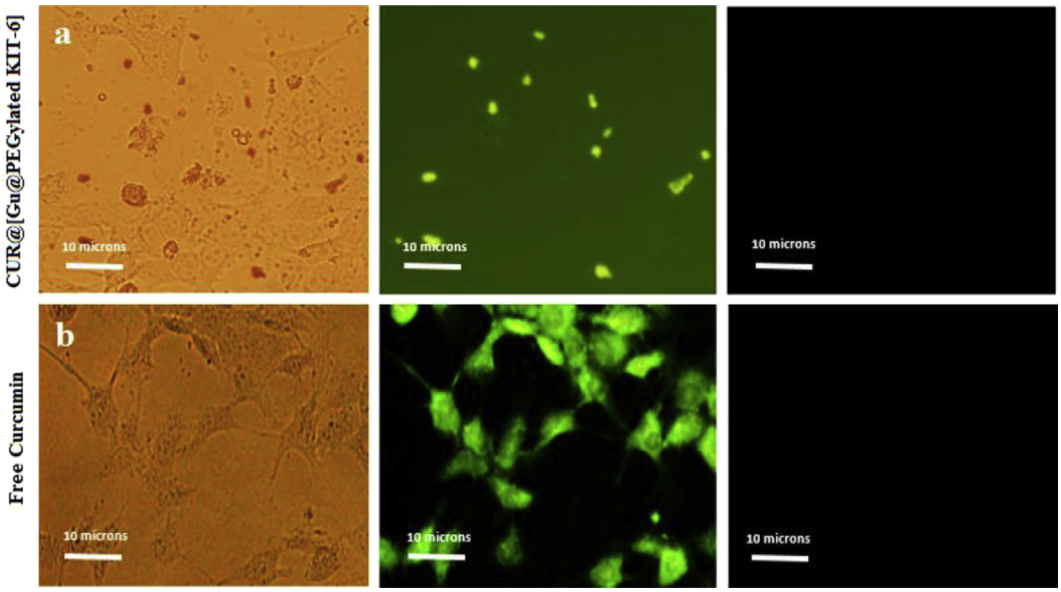

Fig. 10. The intracellular uptake of CUR@[Gu@PEGylated KIT-6]; (a) CUR@[Gu@PEGylated KIT-6] and (b) free CUR were dispersed in PBS to a final concentration of 200 μM and visualized. MCF-7 cells were treated with 15 μM CUR@[Gu@PEGylated KIT-6] or free CUR and checked with light and U.V. microscopy. CUR crystals with different sizes are observed as dark and bright spots under light and U.V. microscope, respectively. CUR@[Gu@PEGylated KIT-6] is observed only under U.V. microscope as dispersed plots especially inside the cells (400× magnification).

dishes and allowed to grow to 50% confluency. Thereafter, the cells were incubated with 15 μM CUR@[Gu@PEGylated KIT-6] as well as free CUR for 4–6 h. The samples were washed twice with PBS before visualizing by fluorescence microscopy. The homogenized feature of CUR@[Gu@PEGylated KIT-6] configuration recognized in images of light and UV microscopy (Fig. 10). Meanwhile, free curcumin aggregated as crystal bodies with different sizes. Also, the absorbance spectrum of CUR@[Gu@PEGylated KIT-6] did not shift in excitation/emission compared to curcumin dissolved in PBS or 1% methanol (data not shown). To evaluate the cell internalization of free curcumin and its nano version, fluorescence microscopy was performed after 5 h of treating with 15 μM CUR@[Gu@PEGylated KIT-6] and free curcumin.

4. Conclusion

There is significant interest to develop novel and efficient DDSs to augment currently available treatment protocols, which may allow decreased side effects and toxicity without compromising therapeutic efficacy. Curcumin is one such potential candidate, and this report presents design and synthesis of a novel and robust nanoporous carrier for the smart delivering of curcumin and investigates its therapeutic activity in the breast cancer. Curcumin loaded [Gu@PEGylated KIT-6] nanoparticles has been prepared and utilized as an efficient and salient anticancer drug delivery system with pH-responsive controlled characteristics and highly programmed release which led to the satisfactory results in the *in vitro* breast cancer therapy. [Gu@PEGylated KIT-6] nanoparticles as a nanoporous carrier have exhibited extraordinarily high loading capacity and loading efficiency about 50% and 100%. Our obtained results depicted that the pure nanoparticles have no cytotoxicity against normal cells. The saliency of the [Gu@PEGylated KIT-6] nanoparticles include biocompatibility, high loading efficiency, controllability, and penetrability make it a robust and noticeable tool for a vast range of potential applications in biomedicine. The applicability of the current systems is currently under investigation in related fields which will be reported in due course.

Acknowledgment

The authors gratefully acknowledge the Research Council of Tehran University of Medical Sciences, INEF (Iran National Elites Foundation), and INSF (Iran National Science Foundation).

Appendix A. Supplementary data

Supplementary data related to this article can be found at http://dx.doi.org/10.1016/j.ejmech.2014.06.069.

References

[1] (a) R.K. Maheshwari, A.K. Singh, J. Gaddipati, R.C. Srimal, Multiple biological activities of curcumin: a short review, Life Sci. 78 (2006) 2081–2087;
(b) H.P. Ammon, M.A. Wahl, Pharmacology of *Curcuma longa*, Planta Med. 57 (1991) 1–7.

[2] S.C. Gupta, S. Patchva, W. Koh, B.B. Aggarwal, Discovery of curcumin, a component of golden spice, and its miraculous biological activities, Clin. Exp. Pharmacol. Physiol. 39 (2012) 283–299.

[3] (a) T. Ak, İ. Gülçin, Antioxidant and radical scavenging properties of curcumin, Chem. Biol. Interact. 174 (2008) 27–37;
(b) O.P. Sharma, Antioxidant activity of curcumin and related compounds, Biochem. Pharmacol. 25 (1976) 1811–1812.

[4] (a) P. Verderio, P. Bonetti, M. Colombo, L. Pandolfi, D. Prosperi, Intracellular drug release from curcumin-loaded PLGA nanoparticles induces G2/M block in breast cancer cells, Biomacromolecules 14 (2013) 672–682;
(b) S. Bhattacharyya, D. Mandal, G.S. Sen, S. Pal, S. Banerjee, L. Lahiry, J.H. Finke, C.S. Tannebaum, T. Das, G. Sa, Tumor-induced oxidative stress perturbs nuclear factor-κB activity-augmenting tumor necrosis factor-α-mediated T-cell death: Protection by curcumin, Cancer Res. 67 (2007) 362–370.

[5] S.K. Sandur, M.K. Pandey, B. Sung, K.S. Ahn, A. Murakami, G. Sethi, P. Limtrakul, V. Madmaev, B.B. Aggarwal, Curcumin, demethoxycurcumin, bisdemethoxycurcumin, tetrahydrocurcumin and turmerones differentially regulate anti-inflammatory and anti-proliferative responses through a ROS-independent mechanism, Carcinogenesis 28 (2007) 1765–1773.

[6] (a) R. De, P. Kundu, S. Swarnakar, T. Ramamurthy, A. Chowdhury, G.B. Nair, A.K. Mukhopadhyay, Antimicrobial activity of curcumin against helicobacter pylori isolates from India and during infections in mice, Antimicrob. Agents Chemother. 53 (2009) 1592–1597;
(b) S.-H. Mun, D.-K. Joung, Y.-S. Kim, O.-H. Kang, S.-B. Kim, Y.-S. Seo, Y.-C. Kim, D.-S. Lee, D.-W. Shin, K.-T. Kweon, D.-Y. Kwon, Synergistic antibacterial effect of curcumin against methicillin-resistant *Staphylococcus aureus*, Phytomedicine 20 (2013) 714–718.

[7] (a) C.V.B. Martins, D.L. da Silva, A.T.M. Neres, T.F.F. Magalhães, G.A. Watanabe, Curcumin as a promising antifungal of clinical interest, J. Antimicrob. Chemother. 63 (2009) 337–339;
(b) O.A.K. Khalil, O.M.M. de Faria Oliveira, J.C.R. Vellosa, A.U. de Quadros, L.M. Dalposso, T.K. Karam, R.M. Mainardes, N.M. Khalil, Curcumin antifungal and antioxidant activities are increased in the presence of ascorbic acid, Food Chem. 133 (2012) 1001–1005.

[8] (a) V. Ravindranath, N. Chandrasekhara, Absorption and tissue distribution of curcumin in rats, Toxicology 16 (1980) 259–265;
(b) V. Ravindranath, N. Chandrasekhara, In vitro studies on the intestinal absorption of curcumin in rats, Toxicology 20 (1981) 251–257;
(c) V. Ravindranath, N. Chandrasekhara, Metabolism of curcumin-studies with [3H]curcumin, Toxicology 22 (1981) 337–344.

[9] (a) S.S. Bansal, M. Goel, F. Aqil, M.V. Vadhanam, R.C. Gupta, Advanced drug delivery systems of curcumin for cancer chemoprevention, Cancer Prev. Res. 4 (2011) 1158–1171;
(b) A.K. Renfrew, N.S. Bryce, T.W. Hambley, Delivery and release of curcumin by a hypoxia-activated cobalt chaperone: a XANES and FLIM study, Chem. Sci. 4 (2013) 3731–3739;
(c) B.B. Aggarwal, C. Sundaram, N. Malani, H. Ichikawa, Curcumin: the Indian solid gold, Adv. Exp. Med. Biol. 595 (2007) 1–75;
(d) B.B. Aggarwal, A. Kumar, A.C. Bharti, Anticancer potential of curcumin: preclinical and clinical studies, Anticancer Res. 23 (2003) 363–398.

[10] (a) F. Tang, L. Li, D. Chen, Mesoporous silica nanoparticles: synthesis, biocompatibility and drug delivery, Adv. Mater. 24 (2012) 1504–1534;
(b) I.I. Slowing, B.G. Trewyn, S. Giri, V.S.-Y. Lin, Mesoporous silica nanoparticles for drug delivery and biosensing applications, Adv. Funct. Mater. 17 (2007) 1225–1236.

[11] (a) T. Yanagisawa, T. Shimizu, K. Kuroda, C. Kato, The preparation of alkyltrimethylammonium-kanemite complexes and their conversion to microporous materials, Bull. Chem. Soc. Jpn. 63 (1990) 988–992;
(b) J.S. Beck, J.C. Vartuli, W.J. Roth, M.E. Leonowicz, C.T. Kresge, K.D. Schmitt, C.T.-W. Chu, D.H. Olson, E.W. Sheppard, S.B. McCullen, J.B. Higgins, J.L. Schlenkert, A new family of mesoporous molecular sieves prepared with liquid crystal templates, J. Am. Chem. Soc. 114 (1992) 10834–10843.

[12] (a) C.-H. Lee, S.-H. Cheng, Y.-J. Wang, Y.-C. Chen, N.-T. Chen, J. Souris, C.-T. Chen, C.-Y. Mou, C.-S. Yang, L.-W. Lo, Near-infrared mesoporous silica nanoparticles for optical imaging: characterization and in vivo biodistribution, Adv. Funct. Mater. 19 (2009) 215–222;
(b) I.I. Slowing, C.-W. Wu, J.L. Vivero-Escoto, V.S.-Y. Lin, Mesoporous silica nanoparticles for reducing hemolytic activity towards mammalian red blood cells, Small 5 (2009) 57–62;
(c) K.M.L. Taylor, J.S. Kim, W.J. Rieter, H. An, W. Lin, W. Lin, Mesoporous silica nanospheres as highly efficient MRI contrast agents, J. Am. Chem. Soc. 130 (2008) 2154–2155;
(d) S.-H. Wu, Y.-S. Lin, Y. Hung, Y.-H. Chou, Y.-H. Hsu, C. Chang, C.-Y. Mou, Multifunctional mesoporous silica nanoparticles for intracellular labeling and animal magnetic resonance imaging studies, ChemBioChem 9 (2008) 53–57.

[13] (a) Y. Cho, R. Shi, R.B. Borgens, A. Ivanisevic, Functionalized mesoporous silica nanoparticle-based drug delivery system to rescue acrolein-mediated cell death, Nanomedicine 3 (2009) 507–519;
(b) S.-H. Kim, J.-H. Park, C.-Y. Lee, Surface-functionalized mesoporous silica nanoparticles as sorbents for BTEX, J. Porous Mater. 20 (2013) 1087–1093.

[14] (a) X. Liu, B. Tian, C. Yu, F. Gao, S. Xie, B. Tu, R. Che, L.-M. Peng, D. Zhao, Room-temperature synthesis in acidic media of large-pore three-dimensional bicontinuous mesoporous silica with Ia3d symmetry, Angew. Chem. Int. Ed. 41 (2002) 3876–3878;
(b) F. Kleitz, S.H. Choi, R. Ryoo, Cubic Ia3d large mesoporous silica: synthesis and replication to platinum nanowires, carbon nanorods and carbon nanotubes, Chem. Commun. (2003) 2136–2137;
(c) Y.-T. Chan, H.-P. Lin, C.-Y. Mou, S.-T. Liu, Ia3d cubic mesoporous silicas using EO17MA23 diblock copolymers made from ATRP, Chem. Commun. (2002) 2878–2879.

[15] A. Vinu, N. Gokulakrishnan, V.V. Balasubramanian, S. Alam, M.P. Kapoor, K. Ariga, T. Mori, Three-dimensional ultralarge-pore Ia3d mesoporous silica with various pore diameters and their application in biomolecule immobilization, Chem. Eur. J. 14 (2008) 11529–11538.

[16] H. Kouchakzadeh, S.A. Shojaosadati, A. Maqhsoudi, E.V. Farahani, Optimization of PEGylation conditions for BSA nanoparticles using response surface methodology, AAPS PharmSciTech 11 (2010) 1206–1211.

[17] E.K.U. Larsen, T. Nielsen, T. Wittenborn, H. Birkedal, T. Vorup-Jensen, M.H. Jakobsen, L. Ostergaard, M.R. Horsman, F. Besenbacher, K.A. Howard, J. Kjems, Size-dependent accumulation of pegylated silane-coated magnetic iron oxide nanoparticles in murine tumors, ACS Nano 3 (2009) 1947–1951.

[18] J. Park, P.M. Fong, J. Lu, K.S. Russell, C.J. Booth, W.M. Saltzman, T.M. Fahmy, PEGylated PLGA nanoparticles for the improved delivery of doxorubicin, Nanomedicine 5 (2009) 410–418.

[19] A.-C. Faure, S. Dufort, V. Josserand, P. Perriat, J.-L. Coll, S. Roux, O. Tillement, Control of the in vivo biodistribution of hybrid nanoparticles with different poly(ethylene glycol) coatings, Small 5 (2009) 2565–2575.

[20] C.S. Fishburn, The pharmacology of PEGylation: balancing PD with PK to generate novel therapeutics, J. Pharm. Sci. 97 (2008) 4167–4183.

[21] U.I. Tromsdorf, O.T. Bruns, S.C. Salmen, U. Beisiegel, H. Weller, A highly effective, nontoxic T1 MR contrast agent based on ultrasmall PEGylated iron oxide nanoparticles, Nano Lett. 9 (2009) 4434–4440.

[22] A.S. Karakoti, S. Singh, A. Kumar, M. Malinska, S.V.N.T. Kuchibhatla, K. Wozniak, W.T. Self, S. Seal, PEGylated nanoceria as radical scavenger with tunable redox chemistry, J. Am. Chem. Soc. 131 (2009) 14144–14145.

[23] B. Thierry, L. Zimmer, S. McNiven, K. Finnie, C. Barbé, H.J. Griesser, Electrostatic self-assembly of PEG copolymers onto porous silica nanoparticles, Langmuir 24 (2008) 8143–8150.

[24] J. Yang, J. Lee, J. Kang, K. Lee, J.-S. Suh, H.-G. Yoon, Y.-M. Huh, S. Haam, Hollow silica nanocontainers as drug delivery vehicles, Langmuir 24 (2008) 3417–3421.

[25] Q. He, J. Zhang, J. Shi, Z. Zhu, L. Zhang, W. Bu, L. Guo, Y. Chen, The effect of PEGylation of mesoporous silica nanoparticles on nonspecific binding of serum proteins and cellular responses, Biomaterials 31 (2010) 1085–1092.

[26] C.L. Lay, H.Q. Liu, D. Wu, Y. Liu, Poly(ethylene glycol)-graft-hollow silica vesicles for drug delivery, Chem. Eur. J. 16 (2010) 3001–3004.

[27] H. Tan, J.M. Xue, B. Shuter, X. Li, J. Wang, Synthesis of PEOlated Fe_3O_4@SiO_2 nanoparticles via bioinspired silification for magnetic resonance imaging, Adv. Funct. Mater. 20 (2010) 722–731.

[28] (a) M. Falahati, A.A. Saboury, L. Ma'mani, A. Shafiee, H.A. Rafieepour, The effect of functionalization of mesoporous silica nanoparticles on the interaction and stability of confined enzyme, Int. J. Biol. Macromol. 50 (2012) 1048–1054.

[29] (a) T.W. Kim, F. Kleitz, B. Paul, R. Ryoo, MCM-48-like large mesoporous silicas with tailored pore structure: facile synthesis domain in a ternary triblock copolymer-butanol-water system, J. Am. Chem. Soc. 127 (2005) 7601–7610;
(b) M. Falahati, L. Ma'mani, A.A. Saboury, A. Shafiee, A. Foroumadi, A.R. Badiei, Aminopropyl-functionalized cubic Ia3d mesoporous silica nanoparticle as an efficient support for immobilization of superoxide dismutase, Biochim. Biophys. Acta 1814 (2011) 1195–1202.

[30] Y.L. Choi, J. Jaworski, M.L. Seo, S.J. Lee, J.H. Jung, Controlled release using mesoporous silica nanoparticles functionalized with 18-crown-6 derivative, J. Mater. Chem. 21 (2011) 7882–7885.

[31] (a) F.Q. Hu, G.F. Ren, H. Yuan, Y.Z. Du, S. Zeng, Shell cross-linked stearic acid grafted chitosan oligosaccharide self-aggregated micelles for controlled release of paclitaxel, Colloids Surf. B. Biointerfaces 50 (2006) 97–103;
(b) K. Buch, T. Peters, T. Nawroth, M. Sänger, H. Schmidberger, P. Langguth, Determination of cell survival after irradiation via clonogenic assay versus multiple MTT assay-A comparative study, Radiat. Oncol. 9 (2012) 71.